ELSEVIER

Computational Materials Science 23 (2002) 225–234

COMPUTATIONAL MATERIALS SCIENCE

www.elsevier.com/locate/commatsci

The dynamics of dislocation interaction with sessile self-interstitial atom (SIA) defect cluster atmospheres

Jianming Huang, Nasr M. Ghoniem *

Mechanical and Aerospace Engineering Department, University of California, Los Angeles, CA 90095-1597, USA

Accepted 1 June 2001

Abstract

The interaction dynamics between dislocations and radiation induced sessile self-interstitial atom (SIA) dislocation loops in FCC metals are investigated. As a result of dislocation line flexibility, its equilibrium configuration is found to be sensitive to the elastic field of nearby SIA dislocation loops. Dislocation line flexibility also influences the critical stress to free trapped dislocations from pinning atmospheres (i.e. the critical resolved shear stress (CRSS)). Calculated CRSS values differ by up to 100% from the estimates of Trinkaus et al. [J. Nucl. Mater. 249 (1997) 91; J. Nucl. Mater. 251 (1997) 172], which are based on cluster forces exerted on static rigid dislocations. The mechanism of dislocation unpinning from random cluster atmospheres is shown to be a consequence of morphological instabilities on the dislocation line. The initial location of the unlocking instability is always associated with regions of minimum line tension in the vicinity of the lowest cluster density. The growth of dislocation shape fluctuations leads to a sequence of unzipping events, freeing the dislocation from the elastic field of cluster atmospheres. The relative critical shear stress to unlock dislocations in FCC metals, (τ_C/μ), is found to be in the range: 0.001–0.002, for random atmosphere cluster densities of 10^{24}–10^{25} m^3, and in the range: 0.0014–0.003, for coherent cluster atmospheres of the same density range. These values are factors of 4–6 smaller than Kroupa's estimates. Implications of these results to the determination of the upper yield point of irradiated FCC metals are discussed.

1. Introduction

The flow stress of materials is achieved when dislocations can move over microstructurally significant distances. Thus, when dislocation motion is inhibited, a higher stress level is required to propagate dislocations within the crystal, and the flow stress is thus increased. In most deforming metals, the impedance of dislocation motion is associated with dislocation multiplication and subsequent interaction with other nearby dislocations. Dislocation immobilization takes place in the form of sessile junctions, or the formation of dislocation dipoles that are stable against further dissociation. This scenario adequately explains work hardening and the elevation of flow stress with further straining of the metal. In some specific and technically important cases, however, the flow stress can be substantially altered by small amounts of

* Corresponding author. Tel.: +1-310-825-4866; fax: +1-310-206-4830.

E-mail address: ghoniem@ucla.edu (N.M. Ghoniem).

0927-0256/02/$ - see front matter
PII: S0927-0256(01)00205-1

impurities, and this is especially evident in body centered crystals (BCC). Moreover, the emergence of an upper yield point in BCC metals results from the interaction of dislocations with interstitial impurities. In some cases of alloyed FCC metals (e.g. copper crystals containing zinc), the upper yield point has also been observed [1]. To explain this effect, Cottrell [2], and Cottrell and Bilby [3] showed that the flow stress at the upper yield point is a consequence of dislocation detrapping from impurity *clouds*, which are attracted to dislocations as a result of elastic interaction between dislocations and impurity atoms.

The stress–strain behavior of irradiated pure FCC metals is characteristically similar to that of unirradiated BCC metals containing impurities. At some critical irradiation dose (e.g. ~0.1 dpa in Cu), an upper yield point is experimentally observed, followed by a drop in the yield strength. Examined TEM samples show that most dislocations are heavily *decorated* by small, sessile interstitial clusters [4]. To explain the experimentally observed yield drop behavior, the cascade-induced source hardening (CISH) model has been proposed [4], in analogy with the "Cottrell" atmosphere concept. It is experimentally observed that grown-in dislocations are decorated with defect clusters, only under cascade damage conditions, and not under electron irradiation (see, for a review [5,6]). Defect cluster mobility and trapping in the stress field of grown-in dislocations was concluded to be the main cause of experimentally observed *decorations*. The atmosphere decorating dislocations in irradiated FCC metals is mainly composed of small, sessile interstitial dislocation loops, produced by coalescence outside the *stand-off distance*. Highly mobile interstitial clusters, which approach the dislocation at closer distances are absorbed into the dislocation core [5,19]. The CISH model was used to calculate the stress necessary to pull decorated dislocations from the atmosphere of loops around them, so that these freed dislocations can act as dislocation sources. Utilizing Kroupa's infinitesimal loop approximation, Trinkaus et al. [5] showed that the increase in the CRSS in irradiated FCC metals is given by:

$$\Delta\tau \sim 0.4\mu(b/L)(R/d)^2, \tag{1}$$

where μ is the shear modulus, b, L, R and d are the Burgers vector, inter-defect distance, defect radius, and stand-off distance, respectively. In these calculations, as in Kropua's original analysis, dislocations were assumed to be rigid. The phenomenon of yield drop was proposed to result from decoration of grown-in dislocations with small clusters or loops of self-interstitial atoms (SIAs) produced in displacement cascades.

Kroupa [7,8], and Kroupa and Hirsch [9], viewed radiation (or quench) hardening to result from the *long-range* elastic interaction between slip dislocations and prismatic loops. In their model of *friction hardening*, the force necessary to move a rigid, straight dislocation on its glide plane past a prismatic loop was analytically estimated to be inversely proportional to the square of the loop distance normal to the glide plane. Using an infinitesimal loop approximation, Kroupa [7] found the stress tensor of a prismatic loop to be of the form:

$$\sigma_{ij} = k_{ij}\mu bR^2/2\rho^3, \tag{2}$$

where k_{ij} is an orientation factor of on order of unity, R is the loop radius and ρ the distance from the loop center. In a rough estimation, this stress was equated to the applied stress at the mid-point between two loops, with the result

$$\Delta\tau/\mu \sim 4bR^2n, \tag{3}$$

where n is the loop density. The hardening effect was also estimated on the basis of the total forces from randomly distributed loops on a moving dislocation, and found as

$$\Delta\tau/\mu \sim 0.17b/l. \tag{4}$$

Kroupa's model [7,8] of dislocation–defect cluster interaction, and its extension by Trinkaus et al. [5], is based on calculations of elastic interaction forces between dislocations and defect clusters in *rigid and static* configurations. Kubin and Kratochvil [20] have recently developed analytical solutions to the problem of interaction between an infinite, rigid dislocation line, and a rigid dipolar loop composed of four linear segments. The dynamics, and hence the exact mechanism, of dislocation detrapping from defect cluster atmospheres cannot be ascertained from these models.

The main goal of the present work is to determine the mechanisms by which dislocations are trapped and detrapped by small sessile SIA dislocation loops close to their glide plane. While Kroupa's theory can guide estimation of the required critical stress to unpin dislocations from nearby dislocation loops, it does not provide precise quantitative details of the interaction dynamics. We aim at explicitly including dynamics of dislocation line deformation during its interaction with dislocation loops. For this, we apply the method of parametric dislocation dynamics (PDD) [10,11], as briefly described in Section 2. Computer simulations for the interaction between expanding Frank–Read (F–R) dislocation loops and sessile SIA clusters is considered in Section 3. We present results which show the influence of isolated SIA clusters on the equilibrium position of dislocations in Section 3.1. The effects of nearby cluster atmospheres on the dynamics of (F–R) dislocation sources is then investigated in Section 3.2. The mechanism by which dislocations are detrapped from cluster atmospheres in the vicinity of the glide plane is analyzed in Section 3.2. The dependence of the CRSS on the cluster density and distance from dislocations will also be assessed. The simple scaling laws for CRSS, given by Eqs. (1) and (3) will be contrasted with results of full-fledged dislocation dynamics computer simulations. Finally, discussions and conclusions are given in Section 4.

2. Dynamics of dislocation interaction with SIA dislocation loops

Recently, a concerted effort has focused on the dynamical behavior of 3-D dislocation ensembles (e.g. [10–17]). These methods embody varying degrees of details for resolving spatial and temporal dislocation–dislocation interactions. In the following, we outline the unique features of our PDD method for calculations of energies, stresses, forces and motion of dislocation ensembles [10,11]. The method provides high fidelity spatial and temporal resolutions, which will be demonstrated in the study of dislocation-defect dynamics in Section 2.

In the PDD method, each slip dislocation loop emanating from F–R sources is segmented into N_s segments (typically, N_s is in the range 7–30 nodes). Each sessile prismatic defect cluster is assumed to be circular, and its elastic field is described by the infinitesimal loop approximation (Eq. (2)) [7]. A segment, i on an F–R dislocation loop is parametrically described by the position vector components $\hat{r}_i(u)$, as

$$\hat{r}_i(u) = \sum_{m=1}^{N_{\mathrm{DF}}} \mathscr{C}_{im}(u) q_m, \tag{5}$$

where $\mathscr{C}_{im}(u)$ are shape functions, dependent on the parameter u $(0 \leqslant u \leqslant 1)$, q_m are generalized degrees of freedom (DOF) for each node, and N_{DF} are the total number of assigned DFs. The velocity of any point on the dislocation line is the time derivative of the position vector components $\hat{r}_i$:

$$V_i = \frac{\mathrm{d}\hat{r}_i}{\mathrm{d}t} = \sum_{n=1}^{N_{\mathrm{DF}}} \mathscr{C}_{in} \frac{\mathrm{d}q_n}{\mathrm{d}t}.$$

The generalized coordinates q_m at each node are the position vector (**P**) for linear segments, the position and tangent vectors (**T**) for cubic splines, and the position, tangent and normal vectors (**N**) for quintic splines, respectively. In the present application, curved segments of slip dislocation loops are represented by cubic splines, and their motion is confined to the glide plane. The stress tensor components are given by the fast sum [10]:

$$\sigma_{ij} = \frac{\mu}{4\pi} \sum_{\gamma=1}^{N_{\mathrm{loop}}} \sum_{\beta=1}^{N_s} \sum_{\alpha=1}^{Q_{\max}} b_n w_\alpha \times \left[\frac{1}{2} R_{,mpp} (\epsilon_{jmn} \hat{r}_{i,u} + \epsilon_{imn} \hat{r}_{j,u}) + \frac{1}{1-v} \epsilon_{kmn} (R_{,ijm} - \delta_{ij} R_{,ppm}) \hat{r}_{k,u} \right], \tag{6}$$

where $R_{,ijk\ldots}$ are successive derivatives of the radius vector connecting a point on the loop and a field point, b_i the components of Burgers vector, and ϵ_{kmn} the usual permutation tensor. For a dislocation loop ensemble, such as the present situation, we use the property of linear superposition. Thus, the fast numerical sum is performed over the following set: quadrature points $(1 \leqslant \alpha \leqslant Q_{\max})$ associated with weight factors (w_α), loop segments $(1 \leqslant \beta \leqslant N_s)$, and number of ensemble loops

$(1 \leqslant \gamma \leqslant N_{\text{loop}})$. The parametric derivatives of the position vector are $\hat{\boldsymbol{r}}_{k,u}$. The equations of motion for the generalized DOF are based on a variational principle for Gibbs free energy, derived from irreversible thermodynamics [11]. The effects of the kinetic energy of moving dislocations are not included in this work.

Let $B_{\alpha k}$ represent the elements of a diagonal resistivity (inverse mobility) matrix (i.e. friction coefficient in two glide and one climb directions). The sum of the Peach–Kohler force, self-force, Peierls lattice friction and climb forces (per unit dislocation line length) is denoted by f_k^t. The effective *generalized force*, f_m on a curved segment is given by: $f_m = \int_0^1 f_i^t \mathscr{C}_{im}(u)|\mathbf{ds}|$, while each *resistivity matrix* element, γ_{mn}, is computed as: $\gamma_{mn} = \int_0^1 \mathscr{C}_{im}(u) B_{ik} \mathscr{C}_{kn} |\mathbf{ds}|$. The global DOF for the entire loop, Q_l can be obtained by solving the set of differential equations given by [11]:

$$\mathscr{F}_k = \sum_{l=1}^{N_{\text{tot}}} \Gamma_{kl} Q_{l,t}. \tag{7}$$

The local segment resistivity matrix $[\gamma_{mn}]$ is added into corresponding global locations in the global resistivity matrix $[\Gamma_{kl}]$, while the force vector is mapped onto a corresponding global vector: $\mathscr{F}_k$. Here, the total number of DOF for the loop are: $N_{\text{tot}} = N_{\text{s}} N_{\text{DF}}$. The global resistivity matrix $[\Gamma_{kl}]$ is also symmetric and banded or sparse. The component Γ_{kl} is zero if the DOF k and l are not connected through a segment. Eq. (7) represents a set of time-dependent ordinary differential equations which describe the motion of dislocation loops as an evolutionary dynamical system. To insure accurate temporal resolution for the dislocation–cluster interaction dynamics, the time-step is dynamically varied to achieve a pre-determined level of relative accuracy in the position and tangent vectors. The actual time-step is dictated by the dislocation mobility, which is quite high in FCC metals [5]. Numerical integrations of the equations of motion are performed by the implicit iterative methods of Gear [18]. Material data used in the present computer simulations are as follows: lattice constant $(a = 0.3615$ nm), shear modulus $(\mu = 45.5$ GPa), Poisson's ratio $(\nu = 0.35)$, and dislocation resistivity $(B = 10^{-5}$–10^{-4} Pa s).

3. Results of numerical simulations

For a systematic understanding of the influence of sessile interstitial clusters on the flow stress of irradiated materials, we investigate the dynamics of dislocation interaction with various SIA cluster configurations and sizes. In the following, defect clusters are assumed to be circular prismatic interstitial dislocation loops situated on planes that are parallel to the glide plane of an F–R source. Henceforth, the term "cluster" will be used for a small prismatic, sessile interstitial loop, which is composed of SIAs. Clusters have Burgers vectors, selected from the set: $\mathbf{b} = \{(a/2)\langle 1\,1\,0\rangle\}$. The Burgers vector of the expanding F–R source is taken as: $\mathbf{b} = (a/2)[\bar{1}\,0\,1]$. The equations of motion for position and tangent vectors are solved for a number of nodes on the expanding source (typically 5–31 nodes), and the shape is re-computed by implicit iterative integration [18] to ensure stability of the solution. In the following, we present computer simulations for the dynamics of defect cluster interaction with dislocations in FCC Cu. Evaluation of cluster forces by the fast sum [10] method with four cubic splines shows that the infinitesimal loop approximation [8] is reasonably accurate. We henceforth use Kroupa's approximation (Eq. (2)) to calculate cluster forces on F–R dislocations.

3.1. The influence of isolated SIA clusters on dislocation equilibrium

To analyze the dynamics of dislocation loop interaction with a random field of defect clusters in the near vicinity of the line, we need to first consider a simpler case for the interaction between an expanding F–R source and isolated SIA dislocation loops. Fig. 1 reveals several features of the interaction dynamics between an expanding F–R source and two prismatic SIA dislocation loops of parallel Burgers vectors and the same radius (100 a). The two clusters are situated above the glide plane, with centers at the locations: $(-100$ a, -1000 a, 100 a) and $(100$ a, -1000 a, 100 a). In Fig. 1(a), the two clusters have $\mathbf{b} = (a/2)[1\,1\,0]$, while the F–R source has $\mathbf{b} = (a/2)[\bar{1}\,0\,1]$. The time

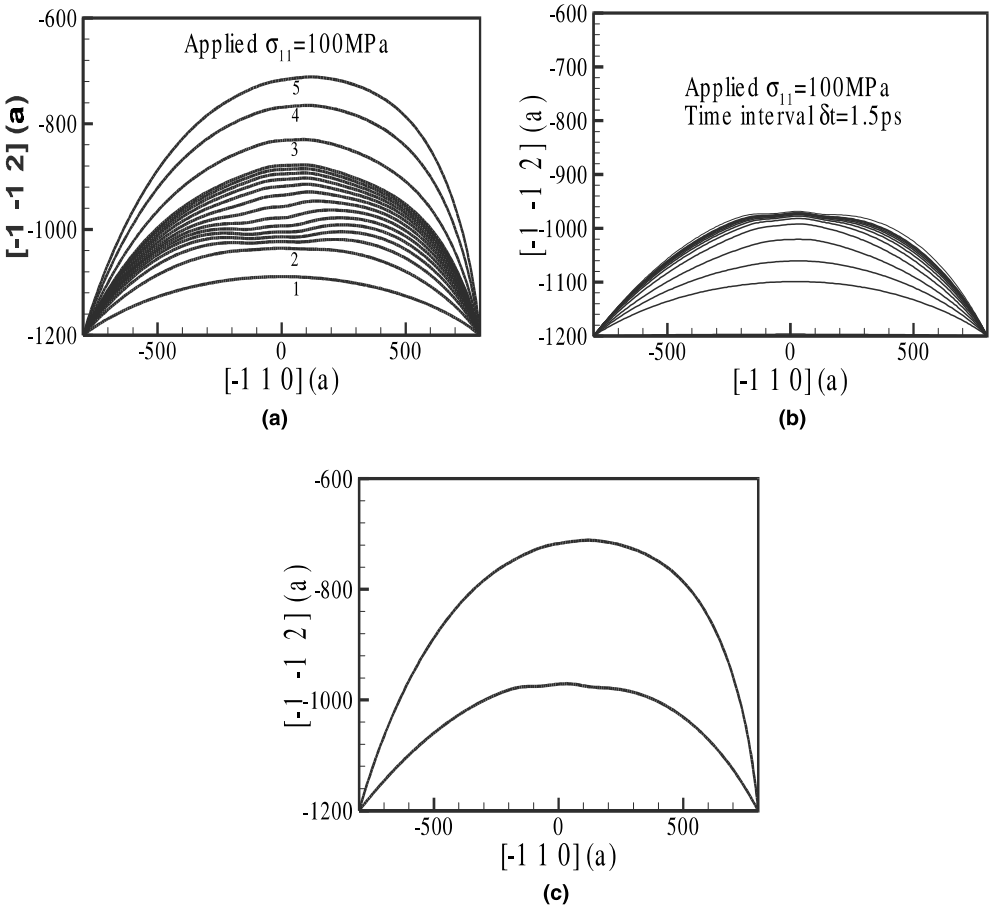

Fig. 1. The influence of two clusters on the deformation of an F–R source with $\mathbf{b} = (a/2)[\bar{1}01]$ in Cu on the (1 1 1)-plane. (a) Two prismatic circular SIA dislocation loops with the diameter of 100 a and $\mathbf{b} = (a/2)[110]$ located in the local position $(-100\text{ a}, -1000\text{ a}, 100\text{ a})$, and $(100\text{ a}, -1000\text{ a}, 100\text{ a})$, time intervals: (1) 1 ps, (2) 4 ps, (3) 52 ps, (4) 75 ps, (5) 150 ps, (6) final equilibrium state. (b) The same SIA dislocation loops with $\mathbf{b} = (1/2)[\bar{1}\bar{1}0]$. (c) Comparison of the final equilibrium states of (a) and (b).

intervals for each dislocation configuration are also indicated in the figure.

The two clusters are initially attractive to the dislocation line because of their Burgers vector orientations with respect to the advancing dislocation. Under the influence of a constant applied stress ($\sigma_{11} = 100$ MPa), however, the F–R source continues its expansion and passes under the two clusters on its glide plane. By about 150 ps, the dislocation reaches an equilibrium configuration with the applied force and its own line tension. The force of the two clusters is too small to play any role at this final stage. The interaction of the same F–R source with two identical clusters to those of Fig. 1(a), except that their Burgers vectors are both given by: $\mathbf{b} = (a/2)[\bar{1}\bar{1}0]$ is shown in Fig. 1(b). When the same stress of σ_{11} is applied in this case, the repulsive forces from the two clusters do not allow the F–R source to penetrate their collective elastic field. Cluster repulsive forces, albeit small, upset the balance between the applied and self-forces on dislocation segments such that the dislocation cannot bypass the cluster, as can be seen from Fig. 1(b). The final equilibrium configuration of the F–R source dislocation is substan#132;tially different in the two cases, as can be ascertained in the comparison shown in Fig. 1(c). Contrary to what might be expected on the basis

of a rigid dislocation approximation, the elastic field of even small clusters can have a dramatic influence on dislocation equilibrium.

3.2. Dislocation interaction with distributions of SIA loops

The complex interaction between an expanding F–R source dislocation and the full field of multiple sessile SIA dislocation loops in a decoration atmosphere is dependent on cluster density, the spatial and size distribution of clusters, and on the orientation distribution of individual Burgers vectors. In an earlier study [21], we showed that dislocation loop unlocking from a row of SIA dislocation loops with parallel Burgers vectors proceeds by development of shape instabilities. We present here an examination of dislocation unlocking dynamics from SIA defect cluster atmospheres. Numerical simulations for the interaction between various limiting SIA defect cluster configurations and an expanding F–R source dislocation will be presented.

In some irradiated BCC metals, coherent SIA dislocation loops in the form of dislocation loop rafts are experimentally observed. Cluster sizes, orientations and spatial distributions appear to be all uniform and the cluster atmosphere is coherent. This limiting case (i.e. fully coherent SIA clusters) will be analyzed. However, most TEM experimental observations of decorated dislocations in FCC metals do not show this high degree of coherence. The other limiting case that will be considered is the case of a random distribution of size, spatial location and Burgers vector of clusters within the atmosphere.

Consider first the interaction between the F–R source and 100 prismatic SIA dislocation loops in an *atmosphere*, which is contained in the parallelepiped bounded by: $(-500\ \mathrm{a} \leqslant x \leqslant 500\ \mathrm{a})$, $(-1015\ \mathrm{a} \leqslant y \leqslant -1000\ \mathrm{a})$, and $(15\ \mathrm{a} \leqslant z \leqslant 30\ \mathrm{a})$. Defect clusters here are assumed to have random Burgers vectors, selected from the set: $\mathbf{b} = \{(a/2)\langle 1\,1\,0\rangle\}$, and are given random locations within the parallelepiped. During the motion of the F–R dislocation, its local curvature changes, thus requiring additional increments in the applied stress to allow continued expansion of the F–R source. Fig. 2 depicts the interaction dynamics between the expanding F–R source and the cluster atmosphere, during the trapping (Fig. 2(a)) and detrapping (Fig. 2(b)) stages. The applied shear stress is increased by 4 MPa intervals, and the dislocation shape is evolved till it reaches an equilibrium configuration, up to the stress level of 36 MPa (Fig. 2(a)). It is noted that the dislocation line shape changes significantly as it approaches the SIA cluster atmosphere. The continuously smooth line, which is determined by the applied stress and line tension, becomes highly curved in the vicinity of the cluster atmosphere. As the applied shear stress increases to a critical value (i.e. the flow stress – which is 40 MPa in this case), the dislocation line flattens and develops incipient fluctuations, as can be seen in (Fig. 2(c)). A morphological shape instability starts in the middle section of the F–R source, when small fluctuations are amplified by applied and self-forces and the dislocation succeeds in penetrating through the collective cluster elastic field. The F–R dislocation loop becomes unstable once it overcomes elastic field of the cluster atmosphere, and would expand till another obstacle is encountered. Details of the interaction dynamics are also shown in Fig. 3, where the 3-D positions of 50 SIA clusters within the atmosphere and the dislocation line position at various time intervals are shown in (a), while the projection of clusters and the dislocation on the glide plane is illustrated in (b). Cluster radii in this atmosphere are in the range: 3–5 a, and their position and Burgers vector are both randomly selected.

The influence of partial or full coherence of the SIA cluster atmosphere on the dynamics of dislocation detrapping is illustrated in Fig. 4(a) and (b), respectively. When the clusters are partially coherent, their size and position is selected randomly, while their Burgers vector (and orientation) are all the same. It is interesting to note that the morphological instability on the F–R dislocation is initiated in the vicinity of the least dense spatial region within the cluster atmosphere, as can be clearly seen in Fig. 4(a). The case of a fully *coherent* cluster atmosphere is illustrated in Fig. 4(b), where the projection of dislocation and cluster positions is shown on the glide plane. Dislocation detrapping from a coherent cluster

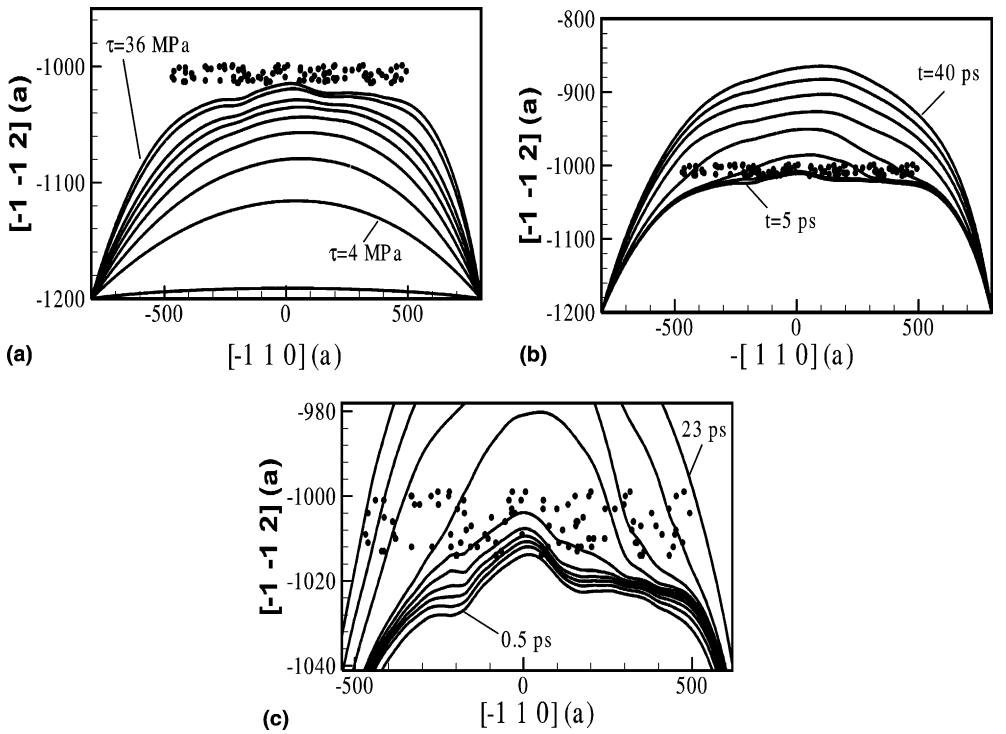

Fig. 2. Dynamics of dislocation *unlocking* mechanism from a cluster atmosphere of 100 randomly distributed sessile SIA dislocation loops (of radius 3–5 a) situated above the slip plane, at stand-off distances in the range: 15–30 a. Their projection on the slip plane is also shown: (a) equilibrium dislocation line configurations at 4 MPa intervals, (b) unstable dislocation configurations at a constant shear stress of 40 MPa and at 5 ps intervals and (c) details of unlocking instability.

atmosphere features spatial asymmetry of the dislocation unlocking instability, as can be seen in Fig. 4(b). This asymmetry results from the high coherence of the cluster elastic field, and the variation of the dislocation line tension with orientation. The dislocation penetrates the cluster atmosphere in a region of minimum line tension, as determined by the F–R dislocation Burgers vector ($\mathbf{b} = (a/2)[\bar{1}\,0\,1]$).

3.3. Scaling of the CRSS with SIA defect clustersize and density

Dependence of the flow stress on the density and size of clusters in decoration atmospheres can be important when one needs to relate the flow stress to the irradiation dose. The results of several computer simulations for the interaction dynamics between a dislocation line and a highly correlated cluster atmosphere are shown as scaling graphs in Fig. 5, together with the scaling relationship of Eq. (1). The relative CRSS (in units of μ) is shown in Fig. 5 as a function of the inverse square stand-off distance, for two fixed inter-cluster spacings (L) of 50 a and 75 a, respectively. For large stand-off distances and inter-cluster spacings, the critical stress is larger than the analytical estimates. This shift in the CRSS in the limit of large stand-off distance above values obtained from Eq. (1) is attributed to the finite length of the F–R source, thus requiring a finite stress to overcome its line tension. On the other hand, computed CRSS at small stand-off distances become significantly smaller than analytical estimates. For small stand-off distances, the dislocation easily unlocks itself by a shape instability, and calculated CRSS values are smaller than analytical estimates. Variations in computed CRSS in Fig. 5 result from the specific statistical distribution of clusters within the atmosphere.

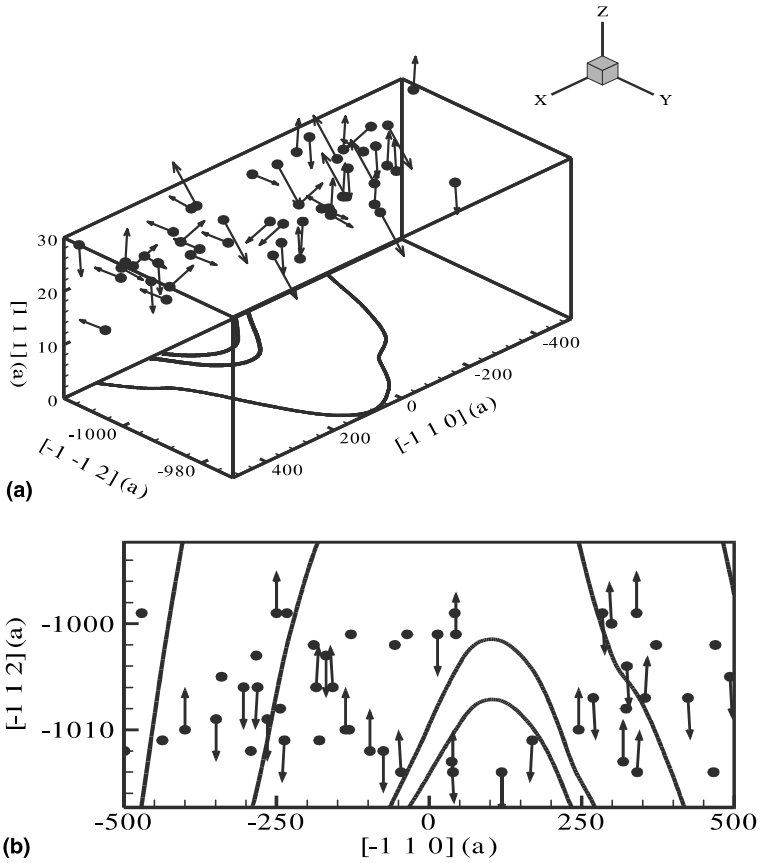

Fig. 3. Closeup for the interaction between an F–R source ($\mathbf{b} = (a/2)[\bar{1}\,0\,1]$) and a random SIA loop atmosphere of 50 sessile SIA dislocation loops near the glide plane. SIA loops have a random distribution of size, space and Burgers vectors: (a) 3-D view and (b) projection on the glide plane.

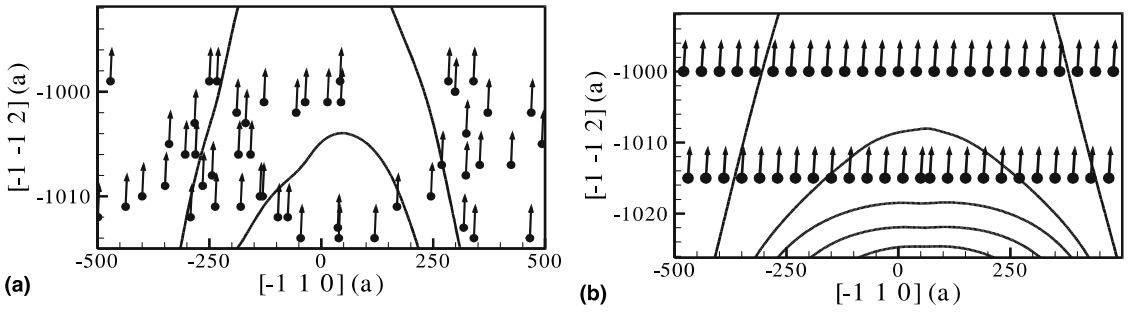

Fig. 4. Interaction dynamics between an F–R source ($b = (a/2)[\bar{1}\,0\,1]$) and a coherent atmosphere of 50 sessile SIA loops near the glide plane. SIA loops have the same size and Burgers vector of $\mathbf{b} = (a/2)[1\,1\,0]$: (a) semi-coherent: SIA loops are randomly spaced and (b) fully coherent: SIA loops are equally spaced.

The influence of the SIA cluster density and coherence on the CRSS is shown in Fig. 6, where the relative value of the CRSS is shown as a function of the local density of SIA clusters within the atmosphere. As one expects, the CRSS increases with the SIA cluster density. However, the

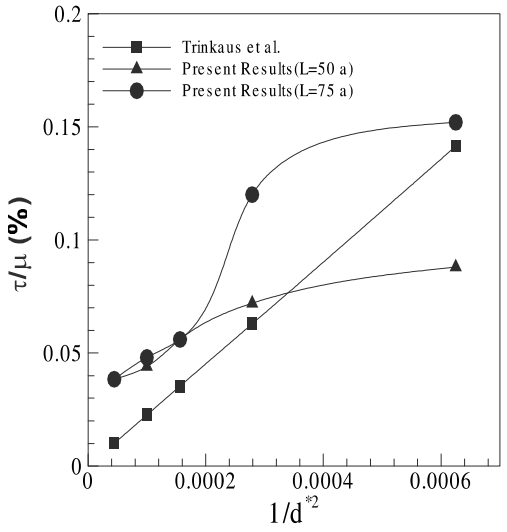

Fig. 5. Scaling relationship for the relative CRSS with the normalized stand-off distance (units of lattice constant), for various fixed inter-SIA loop spacings.

density scaling is dependent on the degree of coherence within the atmosphere, and is not linear for highly coherent SIA cluster atmospheres. The CRSS is higher by about 15–40% for coherent SIA clusters, as compared with random cluster atmospheres. It is important to note that the density scaling expressed by Kroupa's equation (3) is linear, and that it gives results that are a factor of 4–6 *higher* than our current calculations. The discrepancy may be attributed to the rigid, infinite dislocation assumption of Kroupa and the uniform spatial distribution statistics used in his estimate.

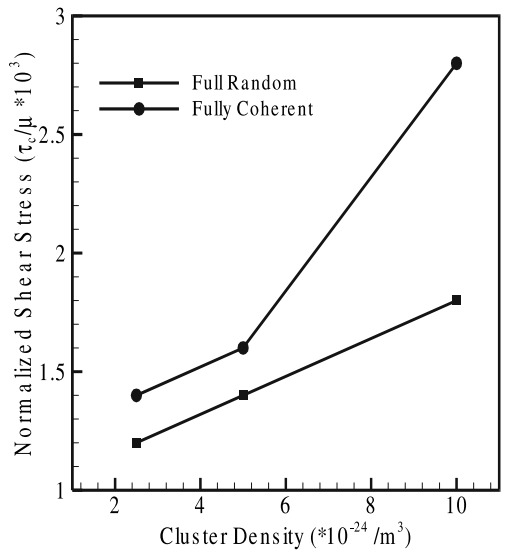

Fig. 6. Dependence of the relative CRSS on the local density of fully random and fully coherent SIA dislocation loops.

4. Conclusions

The mechanism of F–R source dislocation unlocking from this special type of Cottrell-like defect atmosphere (i.e. CISH) has been clarified in the present work. Earlier estimates of the unlocking stress, which are based on the assumption of complete dislocation rigidity during its interaction with SIA dislocation loops do not provide the same scaling of the CRSS with the inter-cluster or stand-off distances. For small inter-cluster or stand-off distances (which are typical of decorated dislocations), the present work shows that the unlocking stress can be a factor of two smaller than values obtained when one assumes rigid dislocation interactions. Two possible mechanisms of dislocation unlocking from highly coherent atmospheres have been identified: (1) shape instability initiated in regions of minimum line tension on the dislocation; (2) shape instability caused by small morphological fluctuations in regions of less-than-average SIA dislocation loop density. The dislocation line first becomes unstable in regions of lowest SIA cluster spatial density. In competition with this driving force is the influence of line tension variation, as the dislocation line itself will have its weakest spots near edge orientations. In cases of high cluster coherence, the unlocking instability is always observed to start on dislocation segments of minimum line tension.

One of the main conclusions of the present study is that the flexibility of dislocations has been grossly underestimated in earlier attempts at deriving scaling laws for the CRSS dependence on SIA cluster density or stand-off distance. As a result of dislocation flexibility, the CRSS is found to deviate substantially from the scaling given by Eq. (1), as well as the Kroupa density scaling, expressed in Eq. (3). While the estimates of these

equations are based on *static* idealized dislocation–cluster configurations, the current computer simulations underscore the critical role of dislocation dynamics in obtaining more precise values. At the root of dislocation unlocking from SIA dislocation loop atmospheres is the initiation of a morphological instability on the dislocation, which propagates to free the line by a sequence of successive unzipping events. It is also clear that the corresponding unlocking stress to free decorated dislocations can be substantially smaller than values obtained on the basis of static calculations alone.

The density and structure of SIA dislocation loops within the decoration atmosphere is difficult to determine experimentally with current TEM methods. However, it is likely that the local SIA dislocation loop density is in excess of 10^{25} m^3. Depending on the degree of coherence within the atmosphere, our simulations indicate that the CRSS may be in the range: 1.8×10^3–2.8×10^3 μ, at a density of 10^{25} m^3. If one considers a polycrystalline Taylor factor of $\sim$3 to determine the corresponding uniaxial stress, the upper yield point in irradiated Cu is estimated to be in the range: 270–420 MPa. Since these values are higher than experimentally observed upper yield points of irradiated Cu [21], it appears that unlocking of heavily decorated dislocations is initiated in areas of stress concentrations (e.g. precipitates, grain boundaries, triple point junctions, or surface irregularities).

Acknowledgements

Research is supported by the US Department of Energy, Office of Fusion Energy, Grant DE-FG03-98ER54500 with UCLA.

References

[1] G.W. Ardley, A.H. Cottrell, Proc. Roy. Soc. London A 219 (1953) 328.
[2] A.H. Cottrell, Report of Conference on the Strength of Solids, University of Bristol England, Physical Society, London, vol. 30, 1948, p. 30.
[3] A.H. Cottrell, B.A. Bilby, Phys. Soc. London 62A (1949) 49.
[4] B.N. Singh, A.J.E. Foreman, H. Trinkaus, J. Nucl. Mater. 249 (1997) 103.
[5] H. Trinkaus, B.N. Singh, A.J.E. Foreman, J. Nucl. Mater. 249 (1997) 91.
[6] H. Trinkaus, B.N. Singh, A.J.E. Foreman, J. Nucl. Mater. 251 (1997) 172.
[7] F. Kroupa, Czech. J. Phys. B 10 (1960) 284.
[8] F. Kroupa, in: B. Gruber (Ed.), Theory of Crystal Defects, Academia Publishing House, Prague, 1966, p. 275.
[9] F. Kroupa, P.B. Hirsch, Discuss. Faraday Soc. 38 (1964) 49.
[10] N.M. Ghoniem, L.Z. Sun, Phys. Rev. B 60 (1999) 128.
[11] N.M. Ghoniem, S.-S. Tong, L.Z. Sun, Phys. Rev. B 139 (1) (2000) 913.
[12] G. Canova, Y. Brechet, L.P. Kubin, in: S.I. Anderson et al. (Ed.), Modeling of Plastic Deformation and its Engineering Applications, RISØ National Laboratory, Roskilde, Denmark, 1992.
[13] B. Devincre, M. Condat, Acta Metall. Mater. 40 (1992) 2629.
[14] J.P. Hirth, M. Rhee, H.M. Zbib, J. Computer-aided. Mater. Design 3 (1996) 164.
[15] L.P. Kubin, Phys. Status Solidi (a) 135 (1993) 433.
[16] K.W. Schwarz, Phys. Rev. Lett. 78 (1997) 4785.
[17] H.M. Zbib, M. Rhee, J.P. Hirth, Int. J. Mech. Sci. 40 (1998) 113.
[18] C.W. Gear, Numerical Initial Value Problems in Ordinary Differential Equations, Prentice-Hall, Englewood Cliffs, NJ, 1971.
[19] N.M. Ghoniem, B.N. Singh, L.Z. Sun, T. Diaz de la Rubia, J. Nucl. Mater 276 (2000) 166.
[20] L.P. Kubin, J. Kratochvil, Philos. Mag. A 80 (1) (2000) 201.
[21] N.M. Ghoniem, S.-H. Tong, B.N. Singh, L.Z. Sun, On dislocation interactions with radiation-induced defect clusters and plastic flow localization in FCC Metals, Philos. Mag. A 81 (11) (2001) 2743.